Journal of Low Temperature Physics (2022) 207:181–189
https://doi.org/10.1007/s10909-022-02711-1

Magnetocaloric Effect for $La_{0.54}Sr_{0.27}Gd_{0.19}MnO_3$ Nanoparticles at Room and Cryogenic Temperatures

Mahmoud A. Hamad[1] · **Hatem R. Alamri**[2]

Received: 21 September 2021 / Accepted: 3 March 2022 / Published online: 9 April 2022

Abstract

The magnetic refrigerator (MR) has gained popularity due to its potential to improve the energy efficiency of refrigeration without the use of unsafe gas, as is the case with traditional gas compression techniques. Magnetocaloric lanthanum manganite investigation, particularly at room and cryogenic temperatures, shows favorable results for the development of MR. Previous thermodynamic models require a significant amount of time and effort to estimate the magnetocaloric effect (MCE). Consequently, we employ the phenomenological model (PM), which is simple and straightforward, requiring fewer parameters than many other modeling methods. We studied the magnetocaloric effect (MCE) of silica-coated $La_{0.54}Sr_{0.27}Gd_{0.19}MnO_3$ (LSGMO) nanoparticles via PM. According to PM results, MCE parameters were obtained as the consequences of the simulated magnetization of silica-coated LSGMO nanoparticles vs. temperature under 0.1 T a magnetic field. It is revealed that the MCE of silica-coated LSGMO nanoparticles covers a broad range of temperatures between 200 and 330 K. The comparison of MCE parameters for silica-coated LSGMO nanoparticles and some published works shows that silica-coated LSGMO nanoparticles are considerably larger than some of the MCE parameters in these published works. Finally, silica-coated LSGMO nanoparticles are suitable function materials in MR, especially at room and cryogenic temperatures, contributing to efficient MR.

Keywords Phenomenological model · Magnetocaloric effect · $La_{0.54}Sr_{0.27}Gd_{0.19}MnO_3$

✉ Mahmoud A. Hamad
m_hamad76@yahoo.com

[1] Basic Science Department, Higher Institute of Engineering and Technology, King Marriott Academy, Alexandria, Egypt

[2] Physics Department, Aljamoum University College, Umm Al-Qura University, Makkah 21955, Saudi Arabia

1 Introduction

Energy efficiency and sustainable development are important issues in modern society. Refrigeration and air-conditioning consume a substantial amount of energy when compared to other uses in both commercial and residential environments [1]. This technology is based on conventional gas compression, which has received considerable criticism for its inefficiency and use of air-polluting gas [1, 2]. Recently, there has been continuous demand to improve magnetic refrigerator (MR) to be a more effective refrigerator than the customary gas refrigeration because MR has high cooling efficiency with low energy consumption, excellent mechanical stability, and low environmental pollution [1–9]. MR relies on the idea of operating magnetocaloric effect (MCE), as a thermomagnetic phenomenon associated with magnetic entropy change (ΔS_M) under an adiabatic magnetic field shift (ΔH) [10–14]. The early development of a gadolinium with a large MCE was a significant starting point in the effort to develop room-temperature MR; however, its use in large-scale commercial applications was severely limited due to its extremely high price [3]. As a result, numerous studies have been conducted in order to find new materials with considerable MCE, high relative cooling power (RCP), and low prices [9, 12–16]. A magnetocaloric material with Curie temperature (T_C) near room temperature and a large ΔS_M over a wide temperature range is of primary interest in designing a MR with operating temperatures nearer to room temperature. It is recommended to develop MR using various categories of magnets in which MCE appears at different temperature ranges, including cryogenic and room temperatures, such as ferrites, manganites, ferromagnetic alloys, magnetic composites, and others [9, 15–18]. There are many considerations in choosing magnetic materials used in the MR industry, such as the broad range of working temperatures with small magnetic hysteresis loss and the low value of their eddy current during the cooling process [19–21]. Recently, manganites have become preferred materials in studying MCE used in MR due to low value of their eddy current and their high resistance to corrosion, with their great chemical stability and ease of preparation [22–24].

Ahmad et al. investigated magnetic and electronic properties of silica-coated $La_{0.54}Sr_{0.27}Gd_{0.19}MnO_3$ (LSGMO) nanoparticles, prepared by the citrate gel method and coated with silica, showing the possibility of using silica-coated LSGMO nanoparticles as restricted hyperthermia without the hazard of overheating in cancer treatment [25]. Furthermore, silica-coated LSGMO nanoparticles have a second-order magnetic phase transition, showing superparamagnetic characterization [25]. This second-order nature with negligible hysteresis loss gives us an expected significant MCE of silica-coated LSGMO nanoparticles over a wide temperature range around T_C. From this significant point, the MCE of silica-coated LSGMO nanoparticles is studied in this work. In this research, a phenomenological model (PM) is considered to study the thermomagnetic properties of silica-coated LSGMO nanoparticles through the simulation of the magnetization–temperature curve for silica-coated LSGMO nanoparticles, concluding (ΔS_M), heat capacity change ($\Delta C_{P,H}$), and RCP.

2 Theoretical Considerations

According to PM, described in [26–28], the magnetization (M) vs. temperature (T) and T_C is given by:

$$M = \left(\frac{M_i - M_f}{2}\right)\left[\tanh(A(T_C - T))\right] + BT + C, \tag{1}$$

where M_i is an initial magnetization at ferromagnetic–paramagnetic transition and M_f is a final magnetization (Fig. 1), $A = \frac{2(B-S_c)}{M_i - M_f}$, B is the average magnetization sensitivity ($\frac{dM}{dT}$) at ferromagnetic state, S_c is the magnetization sensitivity $\frac{dM}{dT}$ at T_C and $C = \left(\frac{M_i + M_f}{2}\right) - BT_C$.

3 Results and Discussion

From experimental data in Ref. [25], we get PM parameters to obtain a characterization of the simulated MCE of silica-coated LSGMO nanoparticles. Figure 2 displays the experimental and simulated isofield magnetization data for silica-coated LSGMO nanoparticles.

From Fig. 2, there is strong convinced conformity between experimental and simulated results of M(T) for silica-coated LSGMO nanoparticles under 0.1 T magnetic field, enhancing the consistency of PM for simulating isofield magnetization. The M(T) curve of silica-coated LSGMO nanoparticles informs us that silica-coated LSGMO nanoparticles show a clear magnetic transition from the ferromagnetic to paramagnetic state over a broad range of temperatures. Consequently, it is expected that the MCE of silica-coated LSGMO nanoparticles covers a remarkable range of

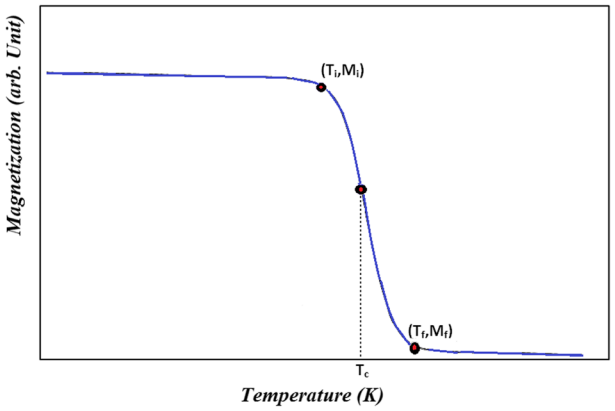

Fig. 1 Magnetization vs. temperature in constant applied field

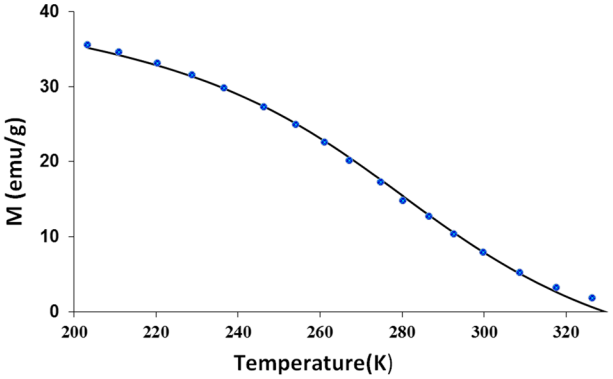

Fig. 2 Magnetization vs. temperature for silica-coated LSGMO nanoparticles in 0.1 T applied magnetic field. The dashed curve is modeled result, and symbols are experimental data from Ref. 25

temperatures, including room temperature. ΔS_M of silica-coated LSGMO nanoparticles under adiabatic ΔH of 0.1 T is given as follows [26–28]:

$$\Delta S_M = 0.1\left(-A\left(\frac{M_i - M_f}{2}\right)\mathrm{sech}^2(A(T_C - T)) + B\right). \tag{2}$$

A maximum of ΔS_M (ΔS_{Max}) can be determined as follows:

$$\Delta S_{Max} = 0.1\left(-A\left(\frac{M_i - M_f}{2}\right) + B\right). \tag{3}$$

Figure 3 shows the simulated of the ΔS_M vs. temperature for silica-coated LSGMO nanoparticles under an adiabatic ΔH of 0.1 T, calculated using Eq. (2). It is clear that the MCE of silica-coated LSGMO nanoparticles covers broadly range of temperatures between 200 and 330 K. This broad range is an approval in MR; especially, it covers room temperature. Furthermore, ΔS_{Max} is 0.04 J/

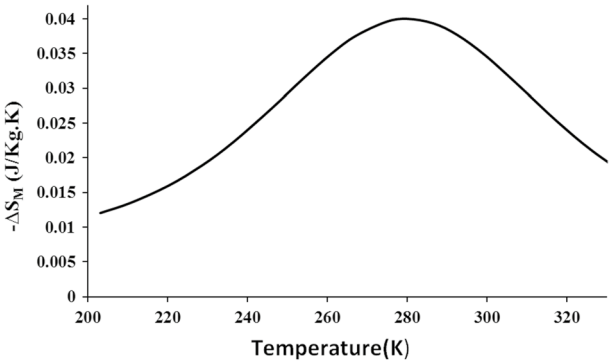

Fig. 3 ΔS_M vs. temperature for silica-coated LSGMO nanoparticles in ΔH of 0.1 T

Kg.K for silica-coated LSGMO nanoparticle which is further than corresponding ones for some MCE material as we will show later. ΔS_M is not the only required parameter to decide the possibility of using silica-coated LSGMO nanoparticles as MCE material in MR. But, there is a request for practical materials of MR to know the RCP parameters that assess the amount of transferred heat at the temperature difference between the hot and cold sinks in the cycle for an ideal MR. RCP is considered by the magnitude of ΔS_{Max} and full-width at half-maximum (δT_{FWHM}) of the ΔS_M curve as follows:

$$\mathrm{RCP} = -\Delta S_{\mathrm{Max}}(T, H_{\mathrm{max}}) \times \delta T_{\mathrm{FWHM}}, \tag{4}$$

where δT_{FWHM} can be obtained as follows

$$\delta T_{\mathrm{FWHM}} = \frac{2}{A}\cosh^{-1}\left(\sqrt{\frac{2A(M_i - M_f)}{A(M_i - M_f) + 2B}}\right). \tag{5}$$

δT_{FWHM} reaches a high value of 116 K at $\Delta H = 0.1$ T. This value of δT_{FWHM} gives a significant practical possibility of using silica-coated LSGMO nanoparticles in MR, since silica-coated LSGMO nanoparticles could function over a temperature range as an effective material for MR, covering a large temperature range below 320 K. RCP of silica-coated LSGMO nanoparticles approximates 4.64 J/Kg at $\Delta H = 0.1$ T.

According to PM model [26], the $\Delta C_{P,H}$ curve of the silica-coated LSGMO nanoparticles is predicted as follows.

$$\Delta C_{P,H} = -0.1TA^2\left(M_i - M_f\right)\mathrm{sech}^2(A(T_{\mathrm{C}} - T))\ \tanh(A(T_{\mathrm{C}} - T)). \tag{6}$$

Figure 4 displays the simulated $\Delta C_{P,H}$ vs. temperature for silica-coated LSGMO nanoparticles under $\Delta H = 0.1$ T. The simulated $\Delta C_{P,H}$ inversely changes from negative value to positive value around T_{C}(Fig. 4), taking values between

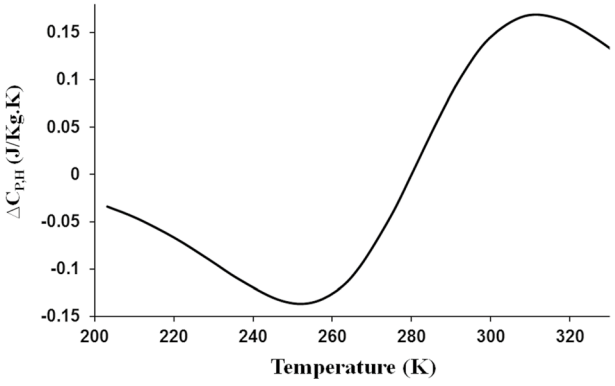

Fig. 4 $\Delta C_{P,H}$ vs. temperature for silica-coated LSGMO nanoparticles in ΔH of 0.1 T

Table 1 Comparison between MCE parameters silica-coated LSGMO nanoparticles and other magnetocaloric materials

Composition	ΔH (T)	$-\Delta S_{Max}$ (J/kg.K)	δT_{FWHM} (K)	RCP (J/kg)	$\Delta C_{P,H(Max)}$ (J/kg.K)	Ref
Silica-coated LSGMO nanoparticles	0.1	0.04	116	4.64	0.168	This work
$Gd_{1-x}Ca_xBaCo_2O_{5.5}$	0.1	1.65E-6—2.2 E-6	9.77—13.85	1.61 E-5—3.04 E-5	6.14 E-5—6.34E-5	[29]
$La_{1.25}Sr_{0.75}MnCoO_6$	0.5	0.0175	26—124	0.45, 2.18	0.04–0.19	[30]
$BiFe_{1-x}Zn_xO_3$	1	0.005- 0.006	4.9–6.9	0.27–0.40	0.022–0.038	[31]
$Ge_{0.95}Mn_{0.05}$ films	0.1	4E-7—3.6 E-6	12.69—17.75	6.3 E-6—0.45E-5	7.7 E-6—1.1 E-4	[32]
Zn0.6Ni0.4Fe2O4	1.7	0.025	–	–	–	[33]
$Ni_{58}Fe_{26}Ga_{28}$	0.2—0.5	0.005—0.013	42—73	0.19—0.94	0.04—0.07	[34]

-0.14 and 0.17 J/Kg.K at $\Delta H = 0.1$ T, causing a variation in the entire specific heat. For additional investigation, the refrigerant capacity (RC) is a valuable parameter to consider the efficiency of silica-coated LSGMO nanoparticle as effective materials in MR. RC was calculated as follows [26–28]:

$$\mathrm{RC} = \int_{T_C - \frac{\delta T_{\mathrm{FWHM}}}{2}}^{T_C + \frac{\delta T_{\mathrm{FWHM}}}{2}} \Delta S_M dT. \tag{7}$$

It is found that RC = 3.41 J/Kg at $\Delta H = 0.1$ T.

Table 1 gives an image of the comparison of MCE parameters for silica-coated LSGMO nanoparticles with the corresponding ones of many MCE materials in published works [29–34]. The MCE parameters of silica-coated LSGMO nanoparticles are considerably larger than some of the MCE parameters of these published works at the same or larger values of ΔH. Finally, silica-coated LSGMO nanoparticles are suitable function materials in MR, especially at room and cryogenic temperatures. The MCE and the electrocaloric effect contribute to modern refrigeration technology perspectives [35–68].

4 Conclusion

According to the thermodynamic calculation via PM, the MCE of silica-coated LSGMO nanoparticles is modeled. It is concluded that silica-coated LSGMO nanoparticles could be operated over a temperature range as a MCE material in MR, covering a large range of practical temperatures, including room and cryogenic temperatures. The PM modeling approach is simple and straightforward, requiring fewer parameters than many other modeling methods. It could be used as part of computational intelligence methodologies for the revealing of new magnetocaloric materials. The superior features of silica-coated LSGMO nanoparticles, such as MCE covering a large range of temperatures below 320 K, and having a low value of eddy current, high resistance to corrosion, great chemical stability, and ease of preparation, make them more favourable for future MR technology.

Funding Open access funding provided by The Science, Technology & Innovation Funding Authority (STDF) in cooperation with The Egyptian Knowledge Bank (EKB).

References

1. Y. Zhang, X. Xu, AIP Adv. **10**, 035220 (2020)
2. Y. Zhang, X. Xu, J. Magn. Magn. Mater. **512**, 166998 (2020)
3. Y. Zhang, X. Xu, RSC Adv. **10**, 20646–20653 (2020)
4. A. Dhahri, E. Dhahri, E.K. Hlil, Appl. Phys. A **116**, 2077 (2014)
5. M.A. Hamad, Process. Appl. Ceram. **11**, 225–229 (2017)
6. M.A. Hamad, J. Supercond. Nov. Magn. **31**, 337 (2018)
7. M.A. Hamad, J. Supercond. Nov. Magn. **27**, 1777 (2014)
8. E.M. Ahmed, O.M. Hemeda, H.R. Alamri, S.M. Elghnam, M.A. Hamad, Phase Trans. **94**, 835–841 (2021)
9. M.A. Hamad, Process. Appl. Ceram. **9**, 11 (2015)
10. E. Zarai, F. Issaoui, A. Tozri, M. Husseinc, E. Dhahri, J. Supercond. Nov. Magn. **29**, 869 (2016)
11. A.M. Ewas, M.A. Hamad, Ceram. Int. **43**, 7660–7662 (2017)
12. A.H. El-Sayed, O.M. Hemeda, M.A. Hamad, A.M. Mohamed, Eur. Phys. J. Plus. **134**, 227 (2019)
13. M.A. Hamad, H.R. Alamri, J Supercond Nov Magn. **35**, 515–518 (2022)
14. M.A. Hamad, J. Supercond. Nov. Magn. **29**, 1539 (2016)
15. A.H. El-Sayed, M.A. Hamad, J. Supercond. Nov. Magn. **32**, 1447 (2019)
16. A.H. El-Sayed, M.A. Hamad, Phase Trans. **92**, 517 (2019)
17. M.A. Hamad, O.M. Hemeda, A.M. Mohamed, J. Supercond. Nov. Magn. **33**, 2521–2525 (2020)
18. M.A. Hamad, O.M. Hemeda, H.R. Alamri, A.M. Mohamed, J. Low Temp. Phys. **202**, 121–127 (2021)
19. M.A. Hamad, O.M. Hemeda, A.M. Mohamed, J. Supercond. Nov. Magn. **33**, 2753–2757 (2020)
20. E.M. Ahmed, H.R. Alamri, S.M. Elghnam, O. Eldarawi, T.E. Tawfik, A.M. Mahmoud, S.E. Elwan, O.M. Hemeda, M.A. Hamad, G.A. Hussein, Phys. Solid State **63**, 1601–1604 (2021)
21. M.A. Hamad, J. Supercond. Nov. Magn. **27**, 2569 (2014)
22. S. Bouzidi, M.A. Gdaiem, S. Rebaoui, J. Dhahri, E.K. Hlil, Appl. Phys. A **126**, 60 (2020)
23. B. Alzahrani, M. Hsini, S. Hcini et al., J. Low Temp. Phys. **200**, 26–39 (2020)
24. C.S. Reddy, C.A. Reddy, A.S. Reddy, P.S. Reddy, Appl. Nanosci. **6**, 461 (2016)
25. A. Ahmad, H. Bae, I. Rhee, AIP Adv. **8**, 015108 (2018)
26. M. Jeddi, H. Gharsallah, M. Bekri, E. Dhahri, E.K. Hlil, J Low Temp Phys. **198**, 135 (2020)
27. M.A. Hamad, J. Supercond. Nov. Magn. **28**, 3111–3115 (2015)
28. M.A. Hamad, J. Adv. Ceram. **4**, 206–210 (2015)
29. M.A. Hamad, Mater. Lett. **82**, 181 (2012)
30. M.A. Hamad, J. Therm. Anal. Calorim. **115**, 523–526 (2014)
31. A.A. Amirov, I.I. Makoed, Y.A. Chaudhari, S.T. Bendre, D.M. Yusupov, A.S. Asvarov, N.A. Liedienov, A.V. Pashchenko, J. Supercond. Nov. Magn. **31**, 3283 (2018)
32. M.A. Hamad, J. Hamad, Supercond. Nov. Magn. **26**, 449 (2013)
33. O.M. Hemeda, N.Y. Mostafa, O.H. Abd Elkader, D.M. Hemeda, A. Tawfik, M. Mostafa, J. Magn. Magn. Mater. **394**, 96–104 (2015)
34. A.H. El-Sayed, M.A. Hamad, J. Supercond. Nov. Magn. **31**, 1895 (2018)
35. M.A. Hamad, Int. J. Thermophys. **34**, 214 (2013)
36. M.A. Hamad, J. Adv. Ceram. **2**, 308–312 (2013)
37. H. El-Sayed, M.A. Hamad, J. Supercond. Nov. Magn. **31**, 4167–4171 (2018)
38. M.A. Hamad, Phase Trans. **86**, 307–314 (2013)
39. M.A. Hamad, J. Supercond. Nov. Magn. **28**, 2525–2528 (2015)
40. M.A. Hamad, J. Supercond. Nov. Magn. **28**, 3365 (2015)
41. M.A. Hamad, J. Supercond. Nov. Magn. **29**, 2867–2871 (2016)
42. M.A. Hamad, Int. J. Thermophys. **34**, 1158–1165 (2013)
43. M.A. Hamad, J. Supercond. Nov. Magn. **28**, 3329–3333 (2015)
44. M.A. Hamad, J. Adv. Dielect. **3**, 1350008 (2013)
45. M.A. Hamad, O.M. Hemeda, H.R. Alamri, M.E. Harb, A.M. Mohamed, Phys. Solid State **63**, 709–713 (2021)
46. A. H. El-Sayed, M.A. Hamad, J. Supercond. Nov. Magn. **31**, 4091–4094 (2018)
47. M.A. Hamad, J. Supercond. Nov. Magn. **29**, 539–1543 (2016)
48. M.A. Hamad, H.R. Alamri, J. Mater. Res. Technol. **17**, 2670–2674 (2022)
49. A. H. El-Sayed, M.A. Hamad, J. Supercond. Nov. Magn. **31**, 3357 (2018)

50. M.A. Hamad, H.R. Alamri, J. Supercond. Nov. Magn. **35**, 515–518 (2022)
51. A. H. El-Sayed, O.M. Hemeda, M.A. Hamad, A.M. Mohamed, J. Supercond. Nov. Magn. **33**, 769–773 (2020)
52. H.R. Alamri, S.M. Elghnam, O.M. Hemeda, M.A. Hamad, Phys. Solid State **63**, 1332–1336 (2021)
53. M.A. Hamad, J. Supercond. Nov. Magn. **27**, 223 (2014)
54. M.A. Hamad, Int. J. Thermophys. **36**, 2748 (2015)
55. M.A. Hamad, O.M. Hemeda, H.R. Alamri, A.M. Mohamed, J. Mater. Res. Technol. **11**, 1356–1361 (2021)
56. M.A. Hamad, J. Comput. Electron. **11**, 344 (2012)
57. M.A. Hamad, J. Adv. Dielect. **3**, 1350029 (2013)
58. M.A. Hamad, H.R. Alamri, M.E. Harb, J. Low Temp. Phys. **204**, 57–63 (2021)
59. M.A. Hamad, O.M. Hemeda, H.R. Alamri, A.M. Mohamed, Phys. Lett. A. **394**, 127204 (2021)
60. M.A. Hamad, J. Supercond. Nov. Magn. **27**, 269–272 (2014)
61. M.A. Hamad, Process. Appl. Ceram. **10**, 33 (2016)
62. M.A. Hamad, H.R. Alamri, Front. Mater. **9**, 832703 (2022)
63. M.A. Hamad, O.M. Hemeda, H.M. Alamri, A.M. Mohamed, J. Supercond. Nov. Magn. **33**, 3853–3856 (2020).
64. M.A. Hamad, H.R. Alamri, Phys. Metals Metallogr. **122**, 1458–1462 (2021)
65. M.A. Hamad, J. Supercond. Nov. Magn. **28**, 2223 (2015)
66. E.M. Ahmed, O.M. Hemeda, H.R. Alamri, S.M. Elghnam, M.A. Hamad, Phys. Metals Metallogr. **122**, 1454–1457 (2021)
67. M.A. Hamad, J. Adv. Dielect. **4**, 1450026 (2014)
68. H.R. Alamri, S.M. Elghnam, O.M. Hemeda, M.A. Hamad, Phys. Solid State **63**, 1332–1336